DETERMINATION OF FRACTURE TOUGHNESS IN PBGA PACKAGES USING FINITE ELEMENT AND EXPERIMENTAL METHODS

by

TAN CHEW PHENG

Thesis submitted in fulfillment of the requirements
for the degree of
Master of Science
U.S.M, Penang

November 2006

14,976 Words

ACKNOWLEDGEMENTS

I would like to express my appreciation and thanks to my supervisor, Assoc. Prof. Dr. Ishak Hj. Abdul Azid and my co-supervisor, Assoc. Prof. Dr. Mani Maran for their grateful support, encouragement and invaluable guidance in helping me to cope in every stage of the project.

I also wish to thank my friends from the School of Mechanical Engineering, Universiti Sains Malaysia especially Mr. Ong Kang Eu and Mr. Lee Boon Leong for their help in this project. I also wish to thank Prof. K. N. Seetharamu and Prof. M. V. V. Murthy for their guidance during the early stage of this project.

I would like to thank every lab staff of the School of Mechanical Engineering especially Mr. Baharom B. Awang and Mr. Md. Ashamuddin Hasim for their technical support during my experiments for this project. I also would like to thank Mr. Md. Zandar Md. Saman from the School of Materials & Mineral Resources Engineering in providing materials.

Finally, I wish to thank my family members for their moral support, especially my parents. Thanks also to those who helped me either directly or indirectly in completing my project.

TABLE OF CONTENTS

Publication List

I.A. Azid, C.P. Tan. B.L. Lee, K.N. Seetharamu (2005). *Fracture Mechanic Analysis for Package Delamination.* Key Engineering Materials, Vols.297-300. p.844-850.

LIST OF TABLES

LIST OF FIGURES

LIST OF PLATES

LIST OF ABBREVIATIONS

		Page
1-D	One-dimensional	8
2-D	Two-dimensional	8,20,22,25-28
3-D	Three-dimensional	20,26,28,52,78-92,121
Ag	Silver	23
Al	Aluminum	51,60-64, 70-77,104-109
Anhyd.	Anhydrides	88
ASTM	American Society for Testing and Materials	55
BSI	British Standards Institute	55
BT	Bismaleimide triazine	22,23,37-40
CCD	Charge-coupled device	83,95
CI	Conventional interferometry	19
C-SAM	C-mode scanning acoustic microscopy	8
CPU	Central processing unit	83
CTE	Coefficient of thermal expansion	15,17
Cu	Copper	17,24,51,60-66,70-75
D.E.R	Dow epoxy resins (trademark of the Dow Chemical Company)	49,77,110-121
DHI	Digital holography interferometry	19,20
EMC	Epoxy molding compound	1-6,16,23,30-34, 77,114-121
ESPI	Electronic speckle pattern interferometry	19
FE	Finite element	3,9,25,30,78

FEA	Finite element analysis	4,9,21-23,29,34,35,40, 45,49,52,59,119,121
FEM	Finite element method	18,25,26
GI	Grating (moiré) interferometry	19
HI	Holographic interferometry	4-7,18-21,68,74-89, 98-107,111-121
IC	Integrated circuit	1,8,9,17
IR	InfraRed	1
JEDEC	Joint Electron Device Engineering Council	40
LED	Light emitting diode	38,39,41,42
LEFM	Linear elastic fracture mechanics	15,25,69
MCCI	Modified crack closure integral	5,24,26,30-32,36,49,119,121
NDT	Non-destructive test	18
PBGA	Plastic ball grid array	2-8,22,23,36-49, 77,114-120
PCB	Printed circuit board	22,23,37-39
PQFP	Plastic quad flat package	53
QFN	Quad flat non-lead	9
RH	Relative humidity	5,22,40-43
SERR	Strain energy release rate	4,15-17,22-27,30, 35,36,45-49,58
Si	Silicon	23,33
SiC	Silicon carbide	49
SIF	Stress intensity factor	4-6,13-17,22-31, 46-53,59,114,118-121
SMD	Surface mount device	7
SMT	Surface mount technology	1,15

SOJ	Small outline J-leaded	40,43
TQFP	Thin quad flat package	5,15,16,32-36,49
VPR	Vapor phase reflow	1,9

LIST OF SYMBOLS

		Page
T_r	Reflow soldering temperature (°C)	2
t_s	Soldering time (s)	2
a_s	Control sample's crack length (m)	6,70-73,106-113
t	Thickness (m)	10-15,26-35,45,52-69, 78,95,98,109,114
F	Applied load (N)	10-14,31,35,45,52-73, 94-99,105-113
δ	Crack edge extension (m)	10-12,55-62,108,112
a	Crack length (m)	10-14,25,26,31-36, 45-73,78,109-114
W	Sample width (m)	10-15,52-73,78, 95,98,109-114
G	Strain energy release rate (J/m^2)	11,12,25,26
U	Stored strain energy (J)	11,12,56,57
C	Compliance, the slope of extension-load (m/N)	12,71-73,108-114
K_C	Critical stress intensity factor (MPa $m^{1/2}$)	12-17,49-54,59-69,74,109,114
G_C	Critical strain energy release rate (J/m^2)	12,15,58,59
E	Young's modulus (GPa)	12,15,23,26,32,33,46, 51-73,94,98,109-114
F_C	Critical loading (N)	12-15,58,59, 70-74,106-114
L	Length distance (m)	13-15,33,52-69,90-113
S	Distance between two pin support (m)	13
K	Stress intensity factor (MPa $m^{1/2}$)	13,14,28

i	Moment inertia of multilayer (dimensionless)	15
E^*	Effective Young's modulus (GPa)	15,32,46
π	Pi (=3.142)	15,25,31,32,46
Ω	Bimaterial constant (dimensionless)	15,31,32,46
J	Crack driving force, J integral (J/m^2)	15,16,27,32,49,53
K_{II}	Mode II stress intensity factor (MPa $m^{1/2}$)	16,26
K_{IIC}	Critical mode II stress intensity factor (MPa $m^{1/2}$)	16
υ	Poisson's ratio (dimensionless)	23,32,33,45, 46,51,62-73
μ	Shear modulus (GPa)	24,31,32,45,46
ψ	Work of the external tractions per unit thickness (J/m)	25
Φ	Strain energy of the body per unit thickness (J/m)	25
σ	Normal stress (N/m^2)	25,29,56
τ	Shear stress (N/m^2)	25,29
v	Opening displacement on crack surfaces (m)	25,26,29,31,35,45
u	Sliding displacement on crack surfaces (m)	25,26,29
G_I	Mode I strain energy release rate (J/m^2)	26,31-36,45-48
G_{II}	Mode II strain energy release rate (J/m^2)	26
K_I	Mode I stress intensity factor (MPa $m^{1/2}$)	26,32,46-49,114
η	Multiplier depending Poisson's ratio υ and geometry (dimensionless) $\eta = 1/(1-\upsilon^2)$ for plane strain; $\eta = 1$ for plane stress	26,46,59
F_y	Normal force (N)	26
F_x	Shear force (N)	26

$\dot{U}$	Strain energy density (J/m^3)	27
$\mathbf{T}$	Traction vector (N/m^2)	27
$\mathbf{u}$	Displacement vector (m)	27
ds	Element of arc length around the contour Γ (m)	27
Γ	Contour in crack driving force (dimensionless)	27
N	Fringe order number (dimensionless)	29,79-81,90-96, 100-107,112
f_p	Optical sensitivity constant (N/m.lines)	29
f_d	Fringe sensitivity (m/lines)	29
B	Additional non-strain-related motion (lines)	29
f_σ	Photoelastic constant for material (N/m.lines)	29
T	Temperature (°C)	29
w	Wetness fraction (dimensionless)	29,40
ρ	Material density (kg/m^3)	29,30,37
k	Thermal conductivity (W/m°C)	29,30,37
D	Moisture diffusivity (m^2/s)	29,30,39
C_{sat}	Saturated concentration (kg/m^3)	29,30,39
C_p	Specific heat (J/kg°C)	29,30,37
P_r	Vapor pressure in the delamination during reflow (Pa)	30,35,43-48
$P_g(T_r)$	Saturation water vapor pressure corresponding to reflow soldering temperature (Pa)	30,38,43
RH_m	Relative humidity at moisture conditioning (dimensionless)	30,43
w_{d,T_r}	Wetness in the delamination during reflow (dimensionless)	30,40,43

κ	Multiplier depending Poisson's ratio υ and geometry (dimensionless) $\kappa=(3-4\upsilon)$ for plane strain; $\kappa=(3-\upsilon)/(1+\upsilon)$ for plane stress	31,32,45,46
l	Length of die pad (m)	33,35,36
e	Length of chip (m)	33,45-48,114
α_T	Thermal diffusivity (m^2/s)	37
h	Convective heat transfer coefficient ($W/m^{2o}C$)	37
w_0	Initial wetness fraction (dimensionless)	40
a_o	Initial delamination length (m)	49
a_C	Allowed length (m)	49
K_{IC}	Plane strain fracture toughness (MPa $m^{1/2}$)	49,51-55,62,66,114
σ_{TS}	Tensile strength (MPa)	51,59-69,110
σ_Y	Yield strength (MPa)	51,54,110
δ'	Total extension (m)	52-56,62,71-73, 78,105-112
δ_C	Critical crack edge (m)	55
ε	Linear strain (dimensionless)	56,106-113
M	External moment (Nm)	56,57
I	Moment inertia (m^4)	56-59,94-98
δ_{z_F}	Deflection at load F (m)	57,58,94-102
q	Distributed load (N/m)	57,58
F_i	Virtual load (N)	57,58
M_i	Virtual moment (Nm)	57,58,94
δ_B	Deflection of beam (m)	58
δ_D	Crack edge enlargement by plate deformation (m)	58

A	Area at the center of thin plate (m^2)	59
$\overline{K_{IC}}$	Mean plane strain fracture toughness (MPa $m^{1/2}$)	60
$\overline{\sigma_Y}$	Mean yield strength (MPa)	60
$K_{IC_{max}}$	Maximum plane strain fracture toughness (MPa $m^{1/2}$)	62,64,69
$K_{IC_{min}}$	Minimum plane strain fracture toughness (MPa $m^{1/2}$)	62,64,69
P	Pressure loading (MPa)	63,65,67
F_T	Tensile loading, 70% less than critical loading (N)	70-74
λ	Laser wavelength (nm)	79-81,90-93,99,103
$\mathbf{i}$	Illumination vector (dimensionless)	79-82,90-94
$\mathbf{o}$	Observation vector (dimensionless)	79-82,90-94
$\mathbf{d}$	Displacement vector (m)	79-81,90-94,99-112
ϕ	Deflection angle (°)	80,90,94
γ	Angle between vector $\mathbf{d}$ and $x-z$ plane (°)	80
PLD	Path length difference (m)	84
L_{obj}	Path length of object beam (m)	84
L_{ref}	Path length of reference beam (m)	84
BR	Beam intensity ratio (dimensionless)	86
I_{ref}	Reference beam intensity (Lux)	86
I_{obj}	Object beam intensity (Lux)	86
θ_o	Observation angle (°)	91,92
θ_i	Illumination angle (°)	91,92,100
θ	Rays angle (°)	92,93,103

β	Rotation angle (°)	93,103
β_{img}	Image turning angle (°)	97,98
x'	Cantilever's coordinate along x' axes (m)	97,98
X	Image pixel along X axes (pixel)	97,98
Y	Image pixel along Y axes (pixel)	97,98
r	Scaling factor along X axes (m/pixel)	98
ξ	Correcting scale for holographic analysis (dimensionless)	105,107,112
δ_o	Initial crack edge (m)	108

LIST OF EQUATIONS

PENGUKURAN KEKUATAN PATAH DALAM PAKEJ PBGA DENGAN MENGGUNAKAN KAEDAH UNSUR TERHINGGA DAN EKSPERIMEN

ABSTRAK

Pakej elektronik khususnya jenis 'plastic ball grid array' (PBGA) mempunyai kegagalan retakan dalaman yang unik yang berlaku disebabkan proses mematerі. Kewujudan kelembapan setempat yang meresap ke dalam pakej menghasilkan tekanan wap. Semasa proses mematerі jenis aliran (215°C), kelembapan yang meresap akan mengewap dan kemudian mengakibatkan retakan 'popcorn'. Oleh itu, kaedah berangka diperlukan untuk memperihalkan rintangan patah dalam bentuk faktor keamatan tegasan (SIF) geometri. Kemudian, kajian ke atas kekuatan patah bahan epoksi sebatian acuan (EMC) menentukan keadaan sempadan untuk retakan pakej.

Dalam kajian ini, perisian Ansys telah digunakan untuk melakukan simulasi taburan kelembapan dan terma demi menentukan tekanan wap pada bahagian retak. Daya tekanan wap ini ditindak ke atas PBGA untuk memperolehi SIF geometri dengan penggunaan kaedah penutupan retak terubahsuai (MCCI). Didapati bahawa kenaikan tekanan wap dan penambahan saiz lekangan menghasilkan SIF geometri yang tinggi. Perhubungan daya-pemanjangan celah retakan yang diperolehi menerusi kaedah holografik interferometri (HI) dan daya kritikal D.E.R. 331 sebagai EMC telah digunakan untuk menganggar kekuatan patah. Kekuatan patah D.E.R 331 ialah 0.488MPa $m^{1/2}$.

Akhirnya, kekuatan patah D.E.R. 331 ini telah dibandingkan dengan SIF geometri untuk PBGA. Graf menunjukkan pelbagai keadaan sempadan

selamat pakej telah diperolehi. Daripada graf ini, boleh disimpulkan bahawa PBGA masih selamat semasa proses mematerі, iaitu tekanan wap 1.21MPa dan nisbah lekangan kurang daripada 0.6. Kegagalan pakej elektronik ini dapat dikawal dengan pengurangan kesan tekanan wap dan lekangan antara permukaan chip dan EMC.

DETERMINATION OF FRACTURE TOUGHNESS IN PBGA PACKAGES USING FINITE ELEMENT AND EXPERIMENTAL METHODS

ABSTRACT

Electronic packages especially the plastic ball grid array (PBGA) has its unique crack failure arising from the soldering process. The existence of moisture absorbed in package from ambient condition causes vapor pressure. During reflow soldering processes (215°C), the moisture absorbed vaporizes and eventually causes popcorn cracking. So, numerical method is used to characterize the fracture resistance in terms of geometric stress intensity factor (SIF). Then, the investigation of fracture toughness on epoxy molding compound (EMC) material provided boundary conditions of package cracking.

In this research, Ansys software was used to simulate moisture diffusion and thermal transfer to determine the vapor pressure at the crack region. The vapor pressure loading was applied on PBGA to obtain geometric SIF using modified crack closure integral (MCCI) method. It was found that the increased in vapor pressure and higher delamination size created high geometric SIF. Load-crack edge extension relation obtained from holographic interferometry (HI) method and critical load for D.E.R. 331 as EMC material were used to evaluate fracture toughness. The fracture toughness for D.E.R 331 was found to be 0.488MPa $m^{1/2}$.

Eventually, the fracture toughness for D.E.R. 331 was compared with PBGA's geometric SIF. A graph with package safety conditions was obtained. From the graph, it can be concluded that the PBGA is typically to be saved during soldering process, where vapor pressure is 1.21MPa and delamination

ratio is less than 0.6. This EP's failure can be controlled through minimizing the effect of vapor pressure and reducing die/EMC interface delamination.

CHAPTER 1

INTRODUCTION

1.1 Background of research

Electronic packaging (EP) designing and manufacturing tend to become a challenging global industry. The challenges emphasize on making the EP lighter, higher packaging density (miniaturization) with the complexity in functions and increased electrical performance while the cost remains at low level. However, these challenges of packaging are hard to achieve and bring difficulties in processing, handling and understanding of smaller components particularly with the use of thinner dies. The matter arising now is how to produce a high reliability EP.

Higher density and more compact developed systems are turning the manufacturers to surface mount technology (SMT) which needs full concern of failure mechanism inside plastic package which is known as popcorn cracking. The package is highly sensitive to moisture and humidity conditions. Its applications mostly include consumer electronics, household appliances, computing, automotive, telecommunications, flight control, robotics, military equipments and astronautics.

Plastic failure usually happens when the moisture diffused in the package during storage becomes vaporized and exerts a pressure known as vapor pressure that could result in the popcorn effect. Wong, E.H. et al. (1998) found that vapor pressure is responsible for the eventual popcorn cracking of plastic integrated circuit (IC) packages during soldering process.

Tay, A.A.O. et al. (1994) mentioned that during soldering by vapor phase reflow (VPR) or infrared (IR) reflow (Figure 1.1) or wave soldering techniques.

the EP is heated up to solder melting temperature in the region of 215°C and exposed to humid environment. High thermal stresses were induced within the EP as the result of enhanced thermal mismatch between dissimilar materials. Meanwhile, the evaporation of moisture caused high stress typically between molding compound (MC) and chip interfaces. These stresses mainly contributed to the phenomenon of cracking inside the EP especially the plastic ball grid array (PBGA) during the reflow soldering process.

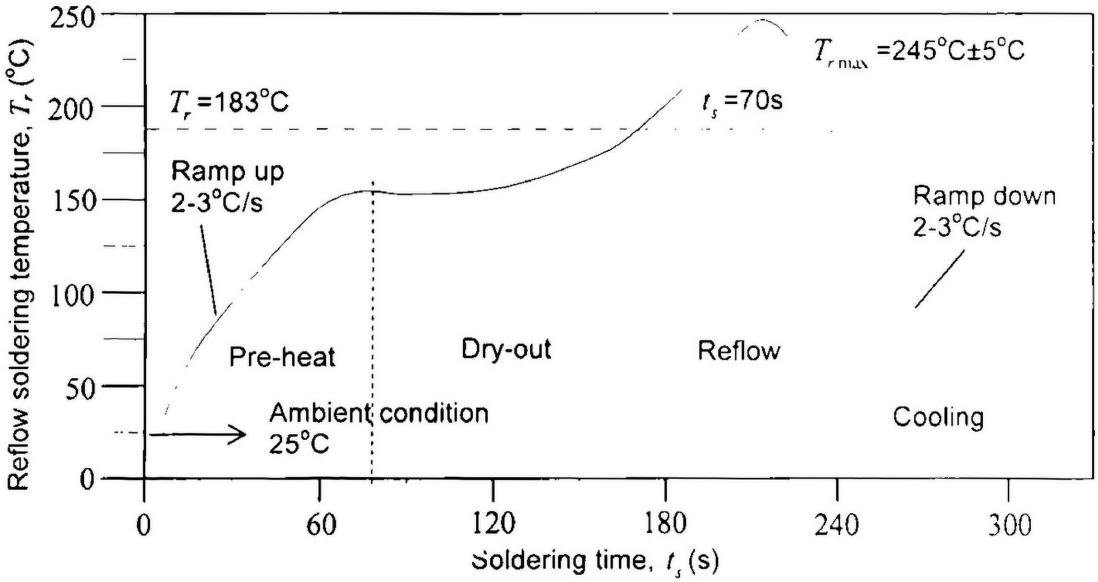

Figure 1.1: IR reflow soldering profile (OSRAM catalog, 2006, p.97)

From these circumstances, it is important to study the micro mechanics of interface delamination and popcorn cracking. Park, Y.B. et al. (1997) noted that the popcorn cracking phenomenon inside the surface mounted packages was known by assuming an inherent edge crack at die pad/epoxy molding compound (EMC) interface and subsequently interface delamination under thermal and vapor pressure loadings. According to Alpern, P. et al. (2002), there were three types of popcorn failure mode in relation to the starting interface of the cracks. Mode I refers to package cracks produced from die pad backside/MC interface delamination, mode II from die attach (DA)/die pad

interface delamination and mode III from chip surface/MC delamination. In 2002, the Hitachi, Ltd. had successfully developed a consistent quality assurance system with specifications and requirements, starting from the planning of development through after sales service to improve the reliability and quality of package device.

The thermal and moisture analysis of EP during soldering process can be done using commercial finite element (FE) software such as Ansys and Nastran to evaluate the package crack phenomenon. Meanwhile, the EMC material crack resistance has being studied using experimental methods such as tensile test and optical methods.

From these studies, the failure of EP could be controlled through the understanding of the effect of thermal transfer, moisture diffusion and humidity during soldering process. The selection of proper MC material with the delamination sizes allowed for the package could also be determined.

1.2 Problem statement

During soldering process, temperature rises rapidly and eventually high stress occurs inside the EP especially PBGA. The tips of delamination between MC and die pad interface become unstable, deform, suddenly collapse and crack propagation at MC region. It is known as fast fracture or plastic collapse (Figure 1.2) as described by Wong, E.H. et al. (2002). Due to these effects, failures such as circuit damage or burn can occur. Thus, the study of fracture toughness on MC material must be applied so that the proper MC material can be selected with the delamination size allowed to prevent plastic collapse.

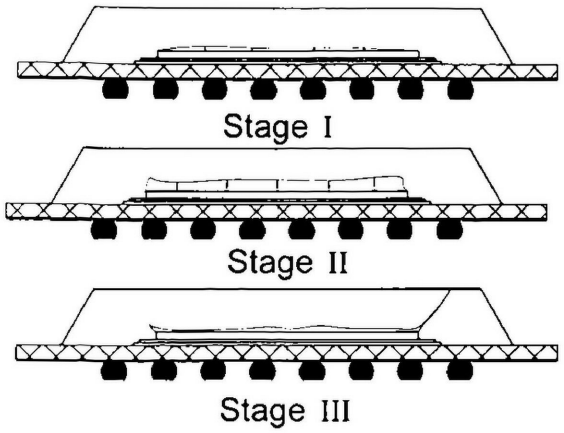

Stage I
- Delamination
- Brittle crack growth into MC

Stage II
- Plastic deformation inhibits crack growth
- Increasing vapor pressure with temperature
- Increase plastic doming

Stage III
- Critical vapor pressure reached
- Plastic collapse occurs
- Pressure release, deflate dome

Figure 1.2: Plastic collapse of popcorn failure (Wong, E.H. et al., 2002, p.228)

1.3 Objectives

Based on the problem, two objectives are identified. They are as follow;

a) To investigate the PBGA failure

The mechanism of popcorn cracking is simulated by using finite element analysis (FEA) and to generate a solution in terms of strain energy release rate (SERR) and stress intensity factor (SIF). Subsequently, the study attempts to find PBGA crack resistance related with vapor pressure and delamination length.

b) To determine the EMC material fracture toughness

The crack edge extension rate with different crack sizes under slow and monotonic increasing loading is obtained using holographic interferometry (HI) method and consequently to determine fracture toughness for EMC material. Eventually, the study attempts to find the PBGA safety conditions on the EMC crack resistance.

1.4 Scope of research

To achieve the two objectives, the study consists of;

a) Modeling popcorn cracking on PBGA for geometric SIF estimation
   - Simulating wetness and temperature distribution under reflow soldering condition (220°C and 85°C/85%RH)
   - Calculating vapor pressure under moisture preconditioning
   - Verifying modified crack closure integral (MCCI) method using TQFP
   - Applying MCCI method on the PBGA to find geometric SIF during reflow soldering

b) Modeling thin plate with center crack to predict fracture toughness
   - Modeling thin plate (100 x 20 x 3mm) in different crack ratio (0.1-0.3)
   - Estimating critical loading on aluminum, copper, mild steel and epoxy
   - Determining compliance rate in different crack ratio
   - Parameter study on fracture toughness to find signification factors such as total extension and crack edge extension, total length, thickness, crack length ratio and applied load

c) Investigating a conventional method known as tensile test on fracture toughness determination
   - Finding critical loading experimentally which is the maximum tensile loading
   - Comparing tensile results with simulation results on aluminum, copper and mild steel

d) Developing an experiment known as HI method for fracture toughness determination.
   - Calibrating HI method using cantilever deflection (1μm-16μm)

- Determining compliance rate in different crack length ratio (0.1-0.3)
- Determining critical loading at crack length, a_s = 4mm using tensile test
- Verifying holographic interferometry fracture toughness test using aluminum plate
- Obtaining EMC material's fracture toughness and compare with material property from findings

e) Comparing facture toughness of EMC material with PBGA geometric SIF to find the safety region in the vapor pressure and delamination ratio condition

CHAPTER 2

LITERATURE REVIEW

2.1 Introduction

Before proceeding with the research analyses and improvements, theoretical and experimental applications from other researchers were studied to understand the main problem of package failure and causes were sought Studies had been carried out by many researchers to explain the vapor pressure effect on the electronic packaging (EP) and to conduct investigation on crack occurrence and resistance usually in molding compound (MC) region. Fracture toughness analysis and holographic interferometry (HI) techniques also were reviewed to understand the development of measurement techniques.

2.2 Review of related research on vapor pressure effect

During soldering, the surface mount device (SMD) was subjected to high thermal stress and vapor pressure induced by moisture diffusion, and eventually developed cracking (Omi, S. et al., 1991) as illustrated in Figure 2.1. Sauber, J. et al. (1994) added that high stress concentration usually occurred at the edge of plastic package's chip and DA in form of local delamination or pre-existing crack.

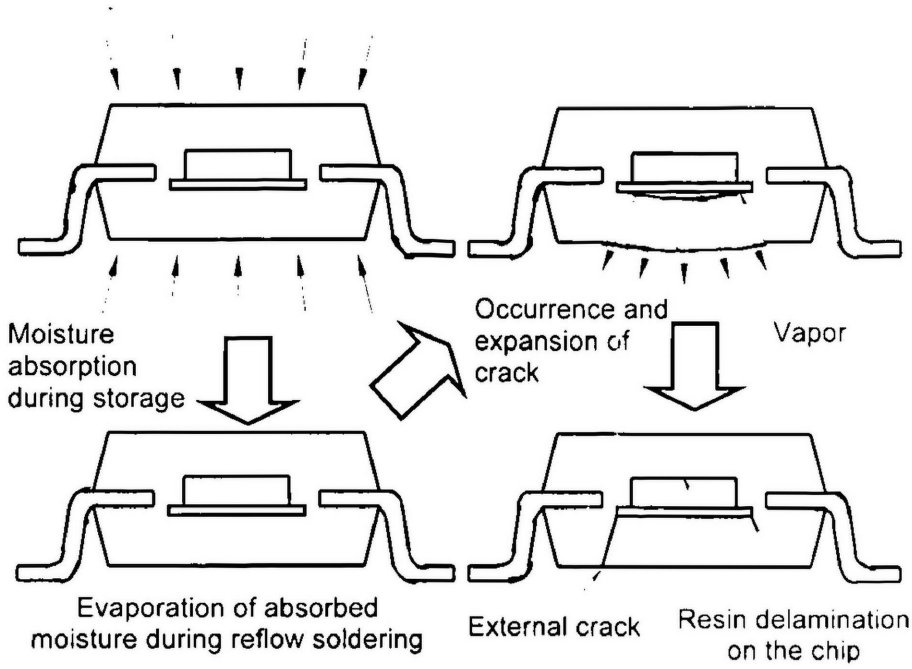

Figure 2.1: Cracking mechanism during reflow soldering (Omi, S. et al., 1991, p.818)

Yip, L. et al. (1996) and Wong, E.H. et al. (1998) found that the amount of moisture absorbed by the package highly influenced it susceptibility to popcorn effect. In another paper by Wong, E.H. et al. (2002), the study proposed a comprehensive solution of moisture induced failure in integrated circuit (IC) packaging including plastic analysis of popcorn cracking. The study introduced a wetness technique for modeling moisture diffusion in multi-layer system such as PBGA during reflow soldering process to overcome the discontinuity concentration on Fick's application.

Tay, A.A.O. et al. (1996) claimed that the simulation of moisture diffusion during reflow in two-dimensional (2-D) is more realistic to the limitations of hitherto one-dimensional (1-D) analysis used by Kitano, M. et al. (1988). Else. Yip, L. et al. introduced another method namely C-mode scanning acoustic microscopy (C-SAM) to investigate the impact of moisture on package delamination and cracking during reflow soldering. The study provided package reliability test.

With the implementation of thermal-moisture analogy and commercial thermal finite element analysis (FEA) software in Tay, A.A.O. et al. (1996) and Wong, E.H. et al. (1998), the finite element (FE) simulation of moisture diffusion during preconditioning of plastic IC package, temperature and moisture diffusion during vapor phase reflow (VPR), and vapor pressure built up in the delamination during VPR had been simulated. Tee, T.Y. et al. (2002) also presented comprehensive modeling on moisture diffusion during preconditioning and reflow process, thermal, hygro-mechanical stress, thermo-mechanical stress and vapor pressure in quad flat non-lead (QFN) package.

Generally, the cracking are divided into three types which are Type I, II and III depending on the origin and the spreading direction of cracks mentioned in Omi, S. et al. The study also found that package structure including chip size, resin thickness on the chip and die pad, lead frame (LF) material, elasticity of die bonding material and test conditions on soldering temperature and moisture absorption ratio were predominant of crack occurrence. Therefore, Omi, S. et al. suggested anti-crack package design through improving MC soldering heat resistance, applying polyimide coating on die pad back side and improving LF design.

In Yip, L. et al. studies did not discuss the moisture conditions that caused cracking nor suggested the solution on reducing moisture absorption rate. The effect of induced vapor pressure in the delamination and crack resistance during reflow were not investigated by Tay, A.A.O. et al. (1996). Wong, E.H. et al. (2002) did not mention the effect of material properties to the moisture induced vapor pressure. Tee, T.Y. et al. did not pointed out the causes of moisture diffusion and vapor pressure to the package plastic failure.

And, the efficiency and capability of the suggested anti-crack design were not clearly analyzed by Omi, S. et al.

2.3 Review of fracture toughness analysis techniques

Many fracture toughness methods had been introduced by researchers to suit various test conditions and specimen geometries. Some fracture toughness methods are as follow;

a) Compliance rate application

By assuming a cracked body (Figure 2.2) with constant thickness, t is subjected to an external load, F and produces a crack edge extension, δ along the path in compliance space.

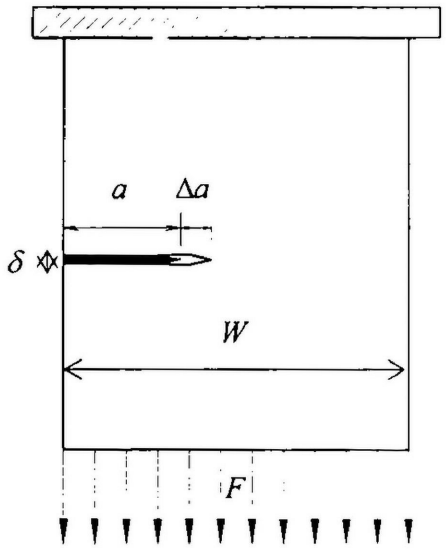

Figure 2.2: Cracked body subjected to load F

The crack extends by an amount of Δa with a corresponding amount of $\Delta\delta$. The whole process is summarized in Figure 2.3.

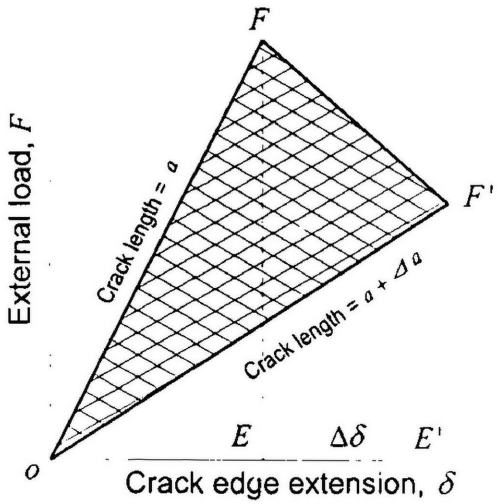

Figure 2.3: Load-extension diagram (Sanford, R.J., 2003, p.245)

According to Sanford, R.J. (2003), energy available for crack edge extension is defined as follow;

$$\begin{aligned} Gtda &= OFF' \\ &= OFE + EFF'E' - OF'E' \end{aligned} \tag{2.1}$$

The area $EFF'E'$ can be approximated by $\partial(F\delta)$, which the work done for crack propagation under external load. However, for constant loading under isolated condition, there is no external work to the system. Difference of area $OF'E'$ with OFE is the total change in stored strain energy (Sanford, R.J.). Thus, it can be simplified as follow;

$$G = \left.\frac{\partial U}{t\partial a}\right|_F \tag{2.2}$$

Where,

U Stored strain energy (J)

For linear elastic condition (Sanford, R.J.),

$$U = \frac{1}{2} F \cdot \delta \tag{2.3}$$

The compliance is defined as,

$$C = \frac{\delta}{F} \tag{2.4}$$

Where,

C Compliance, which is the slope of extension-load (m/N)

Substituting Equation 2.4 into 2.3, it gets,

$$U = \frac{1}{2}CF^2 \tag{2.5}$$

Differentiating with a constant load, it gives,

$$\partial U = \frac{1}{2}F^2 \partial C \tag{2.6}$$

Thus, by substituting Equation 2.6 into 2.2, it gets,

$$G = \frac{F^2}{2t}\left(\frac{\partial C}{\partial a}\right) \tag{2.7}$$

Where,

$\frac{\partial C}{\partial a}$ Compliance rate with crack length (1/N)

These can be applied on any geometrical shapes under a monotonic increasing loading with constant thickness. It can be extended to determine fracture toughness,

$$\begin{aligned} K_C &= \sqrt{G_C E'} \\ &= \sqrt{\frac{F_C^2}{2t}\left(\frac{\partial C}{\partial a}\right)E'} \end{aligned} \tag{2.8}$$

Generally, this application was basically taken by researchers to develop a standard method. In this study, it was used to determine fracture toughness for an epoxy based polymer.

b) Single edge notched bend (SENB) or three point bend (3PB) test

In SENB (Figure 2.4), stress intensity factor (SIF) depends on applied load, F and sample geometry.

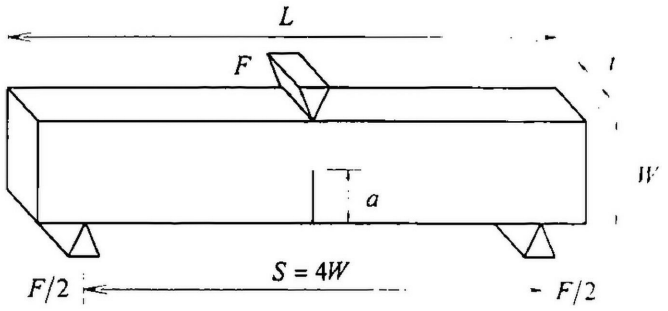

Figure 2.4: SENB for K determination

The SIF is given by Anderson, J.C. et al. (1991) as follow;

$$K = \frac{3FS}{2tW^{3/2}}\left[1.93\left(\frac{a}{W}\right)^{1/2} - 3.07\left(\frac{a}{W}\right)^{3/2} + 14.53\left(\frac{a}{W}\right)^{5/2} - 25.11\left(\frac{a}{W}\right)^{7/2} + 25.8\left(\frac{a}{W}\right)^{9/2}\right]$$
$$= \frac{6F}{tW^{1/2}}\left[1.93\left(\frac{a}{W}\right)^{1/2} - 3.07\left(\frac{a}{W}\right)^{3/2} + 14.53\left(\frac{a}{W}\right)^{5/2} - 25.11\left(\frac{a}{W}\right)^{7/2} + 25.8\left(\frac{a}{W}\right)^{9/2}\right]$$
$$= \frac{F}{tW^{1/2}}\left[11.58\left(\frac{a}{W}\right)^{1/2} - 18.42\left(\frac{a}{W}\right)^{3/2} + 87.18\left(\frac{a}{W}\right)^{5/2} - 150.66\left(\frac{a}{W}\right)^{7/2} + 154.8\left(\frac{a}{W}\right)^{9/2}\right] \quad (2.9)$$

Where,

S Distance between two pin support (m)

As the load increases, SIF will increase accordingly. The crack will start to propagate when critical load, F_C is reached. So, the fracture toughness is given by Smith, R.N.L. (1991) as follow;

$$K_C = \frac{F_C}{tW^{1/2}} \cdot f\left(\frac{a}{W}\right) \quad (2.10)$$

Where,

$$f\left(\frac{a}{W}\right) = \left[11.58\left(\frac{a}{W}\right)^{1/2} - 18.42\left(\frac{a}{W}\right)^{3/2} + 87.18\left(\frac{a}{W}\right)^{5/2} - 150.66\left(\frac{a}{W}\right)^{7/2} + 154.8\left(\frac{a}{W}\right)^{9/2}\right]$$

c) Compact tension (CT)

In CT (Figure 2.5), SIF also depends on applied load, F and sample geometry.

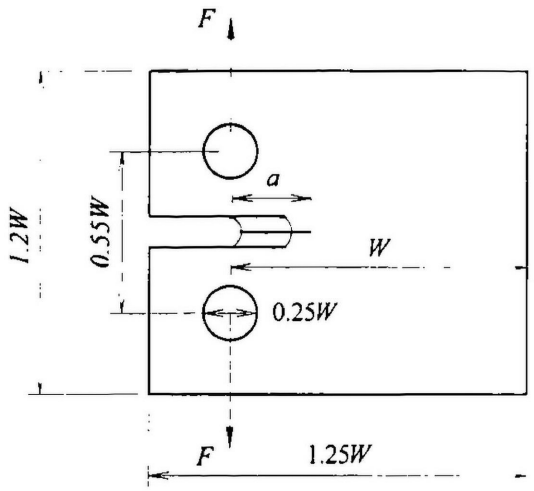

Figure 2.5: CT for K determination

The crack will propagate when critical load, F_C is reached. So, the fracture toughness is given by Smith, R.N.L. (1991) as follow;

$$K_C = \frac{F_C}{tW^{1/2}} \cdot f\left(\frac{a}{W}\right) \tag{2.11}$$

Where,

$$f\left(\frac{a}{W}\right) = \left[177.6\left(\frac{a}{W}\right)^{1/2} - 1113\left(\frac{a}{W}\right)^{3/2} + 3934.2\left(\frac{a}{W}\right)^{5/2} - 6102\left(\frac{a}{W}\right)^{7/2} + 3833.4\left(\frac{a}{W}\right)^{9/2}\right]$$

d) Four point bend (4PB) test

4PB (Figure 2.6) was used to determine interfacial fracture toughness, referred as the critical SIF when bi-material interface begins to delaminate.

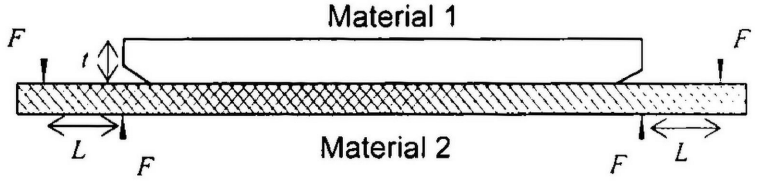

Figure 2.6: Interfacial fracture toughness test

The critical strain energy release rate (SERR) can be determined (Hutchinson, J.W. et al., 1992 and Ferguson, T.P., 2004) as follow;

$$G_C = \frac{1}{2E'_1}\left(\frac{12}{t_1^3}\left(\frac{F_C L}{W}\right)^2\right) - \frac{1}{2E'_2}\left(\frac{12}{it_1^3}\left(\frac{F_C L}{W}\right)^2\right) \tag{2.12}$$

Thus, the interfacial fracture toughness,

$$K_C = \sqrt{G_C E^*}\cosh(\pi\Omega) \tag{2.13}$$

2.4 Review of related research on fracture toughness method

Tay, A.A.O. et al. (1994) classified the primary stress components in the crack tip region into three modes of cracking based on Irwin approach, which were Mode I - opening mode, Mode II - forward shear mode and Mode III - anti plane shear mode. Park, Y.B. et al. (1997) found that the stress states near the crack tip were closer to Mode II for thermal loading and vapor pressure loading in Mode I, but for the mixed loading it changed from Mode II to Mode I.

Therefore, Ganesan, G.S. et al. (1993) developed a quantitative model describing the cracking in surface mount technology (SMT) plastic package to predict crack resistance related with package geometry, MC properties and storage/reflow conditions. Sauber, J. et al. (1994) used linear elastic fracture mechanics (LEFM) to investigate fatigue crack propagation of plastic package under continually thermal loading conditions. Thin quad flat package (TQFP) model with crack in the MC region at the corner of the die pad used J integral application to evaluate the effect of coefficient of thermal expansion (CTE) mismatches, initial crack sizes and die pad delamination.

Park, Y.B. et al. studied the popcorn cracking phenomenon in a surface mounted package, TQFP using ABAQUS finite element code with eight-noded isoparametric element and J integral to calculate SERR of die pad/EMC interface delamination under thermal loading, vapor pressure loading and mixed loading.

Apart from that, Sauber, J. et al. carried out a SENB test to investigate critical SIF, K_c of MC materials. Tay, A.A.O. et al. (1994) proposed a adhesion test (Figure 2.7) and found that delamination begins if the K_{II} in the package exceeded critical value, K_{IIC}.

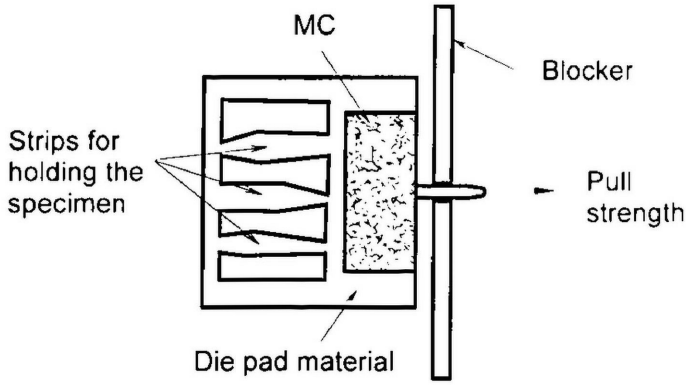

Figure 2.7: Schematic diagram of adhesion test
(Tay, A.A.O. et al., 1994, p.203)

Yeung, B. et al. (2003) established three experiment methodologies to measure die strength in variety of die sizes upon the defects that resulted from processing and handling. Three point bend (3PB) test measured the strength with respect to the backside condition of the die. Four point bend (4PB) test investigated bending conditions for the largest defects namely edge defects caused by wafer sawing or singulation damage. Ball breaker test measured die strength with respect to surface condition and sensitively to edge condition.

Monotonic and cyclic loadings interfacial delamination onset and propagation were studied using experiment test and numerical analysis by Xie. W.D. et al. (2003).

Mercado, L.L. et al. (2003) studied on copper (Cu)/low-k structure for advanced integrated circuits (ICs) to understand its impact properties Multi-level, multi-scale sub-modeling technique was used in the study due to the significant difference in scale between the package and Cu/low-k structures. Interface fracture mechanics method had been adopted to predict interface delamination that occurred in the Cu/low-k stack.

In Sauber, J. et al., the studies found that the K_c values decreased as the temperature decreased, suggesting that cracks tends to propagate more easily at low temperature. On the same time, the K_c values decreased with the increased of mechanical loading rate and thermal loading rate. The studies also showed that the MC with lower CTE reduced the stress intensity factor (SIF) and that SIF increased with the crack size.

Generally, the interfacial delamination aspect to the package cracking was not included in Ganesan, G.S. et al. (1993). Sauber, J. et al. did not discussed the vapor pressure effect that also contributed to crack occurrence. Cracking caused by vapor pressure also did not mentioned by Tay, A.A.O. et al. (1994) and Mercado, L.L. et al. Park, Y.B. et al. did not persist to find geometric SIF which more practical and material independent, apparently the SERR was material and geometry dependent. Yeung, B. et al. did not relate the die strength to package crack occurrence. Xie, W.D. et al. only assumed that interfacial delamination tends to propagate rather than developed cracking at MC region because weak of interface adhesion strength.

2.5 Review on holographic interferometry techniques

Holographic interferometry (HI) method was discovered and developed after Powell and Stetson had attempted in making a hologram (Gryzagoridis. J. 2002). Basically, HI method is based on the interference from the reconstruction of holographic wave fronts, as shown in Figure 2.8.

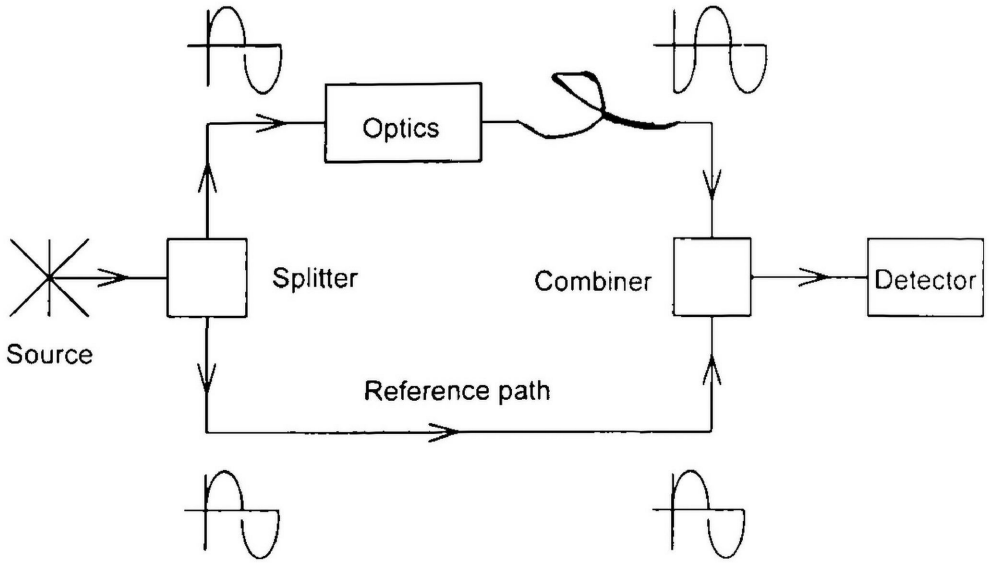

Figure 2.8: Generic interferometry model (Cloud, G.L., 1998, p.39)

In the process of analyzing structure deformation in micrometers or even nanometers scales, HI method was found to be important for designing optimization, particularly the selection of material in electronic packaging (EP) which required accurate knowledge of the behavior of component under actual operating condition. The conventional experiment procedures such as strain gauges, tensile test, photo-elasticity and finite element method (FEM) were lack of persistent in natural. In other words, it is lack of sensitivity in the control environment and lack of flexibility of test (Pryputniewicz, R.J., 1995).

HI method is important for non-destructive test (NDT) in measuring small static displacements and deformations of optical rough surfaces caused by thermal or mechanical loading. It was also used in vibration and modal

analysis, structural analysis, composite materials and adhesive test, stress and strain evaluation, flow, volume and thermal analysis (Fein, H., 1997).

Generally, there are three types of HI techniques which are real-time, multi-exposure and time-average. Real-time interferometry makes a single-exposure hologram of an undisturbed object. After processing, the hologram refits in its precise original position. When the object is subjected to a load, subsequently it produces live fringes. Multi-exposure interferometry creates a hologram by two or sometimes more exposures. Time-average interferometry is used in analyzing the behavior of mechanical system which is vibrating in a stable condition (Saxby, G., 1991).

2.6 Review of holographic technique applied for fracture toughness

Conventional techniques involving strain gauges, photo-elasticity and mechanical probing were generally not applicable to micro-scale component analysis. Alternatively, conventional interferometry (CI), electronic speckle pattern interferometry (ESPI) and shearography, grating (moiré) interferometry (GI), digital holography interferometry (DHI) supported by thermovision and optical, confocal, scanning electron or atomic force microscopy were proposed (Salbut, L. et al., 2001).

Salbut, L. et al. was given some brief and general features on the conceptual and methodology of some useful holographic techniques. Particularly, the CI method used for shape and out-of-plane displacements. ESPI allowed in-plane and out-of-plane displacements measurement of scattering surfaces. While GI used for in-plane displacements and material properties determination of micro-element with surface periodic structure and

DHI provided all components of displacement vector on reflecting and scattering surfaces.

Using holographic interferometry (HI) method, Pryputniewicz, R.J. (1995) presented the study on displacements and strains of small components. The studies also showed quantitative interpretation of hologram for vibrating and thermal loading component. As well, Takao, S. et al. (2002) proposed an optical system using lensless Fourier transformed holographic interferometry to measure in-plane and out-of-plane displacements on beam bending, three point bend (3PB) and thermal deformation, in the range of 5-10μm.

Overall, Pryputniewicz, R.J. only concentrated on determining out-of-plane displacements but actually it can be extended to 2-D or even 3-D displacements. So, the HI optical set-up can be modified to determine strain on uniform axial load system for fracture toughness determination.

2.7 Summary

From the literature survey, it was observed that many researchers had carried out investigations to understand the behavior of crack propagation using different approaches and methods. Based on the literature survey, several features can be concluded as below;

a) Most of the analyses had identified the vapor pressure induced crack including the effect and type of cracking during reflow soldering. The studies also generally suggested some anti-crack solutions. But, most of the analyses did not give clear safety region or boundary conditions for the package to avoid failure.

b) Most of the analyses only concentrated on specific types of package with the used of complicated FEA application. So, the obtained results can only be referred to certain package and may not be applied directly to other types of package.

c) Holographic interferometry (HI) method was applied on the study of displacements and deformations. Most of the works carried out with complicated theories and complex optical arrangement. However, HI method can be modified to determine strain on uniform axial load system for fracture toughness evaluation.

CHAPTER 3

ANALYSIS OF STRESS INTENSITY FACTOR IN PLASTIC BALL GRID ARRAY (PBGA)

3.1 Introduction

The mechanism of popcorn cracking in plastic ball grid array (PBGA) were investigated using finite element analysis (FEA) and the solution in terms of strain energy release rate (SERR) and stress intensity factor (SIF) were generated. Subsequently, the study attempts to find the package crack resistance related with vapor pressure and delamination ratio.

The package was simulated in the condition when it was heated up to 220°C during reflow soldering process under moisture condition 85°C/85% relative humidity (RH) for 5 minutes as described by Ganesan, G.S. et al. (1993). Delamination between molding compound (MC) and die (chip upper surface) was initiated near the die tip location. Ganesan, G.S. et al. proposed that the delamination location was under high vapor pressure after the package was heated from room temperature, 25°C, to solder melting temperature, 215°C. However, cracking was not occur immediately, it happened when the moisture was absorbed into the PBGA became vaporized and exerted a critical vapor pressure.

The PBGA was modeled in two dimensional (2-D) and a ¼ model was taken because the package was symmetry as shown in Figure 3.1.

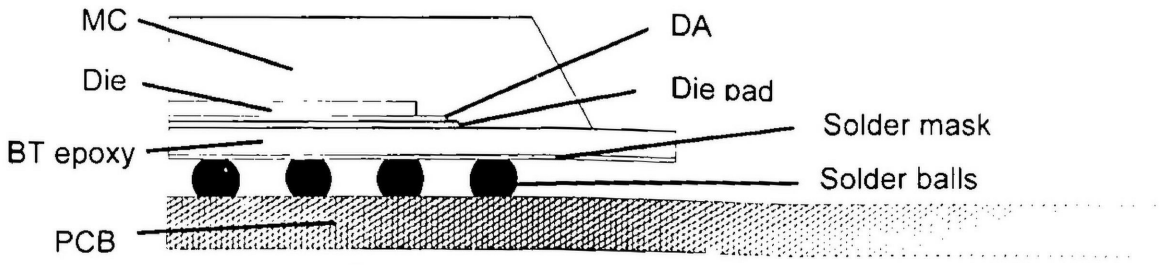

Figure 3.1: Schematic of ¼ PBGA

The package consists of epoxy molding compound (EMC), silicon (Si) die or chip, silver (Ag) filled epoxy die attach (DA), die pad, bismaleimide triazine (BT) epoxy or substrate, solder mask, solder balls or bumps and printed circuit board (PCB). Table 3.1 below shows the specifications of PBGA. The material properties required for FEA are provided in Table 3.2 and 3.3.

Table 3.1: Dimensions of PBGA (Habib Abul Mustain, 1997, p.34)

Package size	16.55 x 18.08mm
Package thickness	2.25mm
Chip size	8.00 x 8.00mm
Chip thickness	0.25mm
DA thickness	0.05mm
Die pad thickness	0.15mm
BT epoxy thickness	0.40mm
Solder mask thickness	0.075mm
Solder balls Diameter Height	 0.75mm 0.60mm
PCB thickness	0.80mm

Table 3.2: Material properties for the main constituents of PBGA (Habib Abul Mustain, 1997, p.49)

Material	Young's modulus, E (GPa)	Poisson's ratio, υ
MC	16.0	0.25
Die	131.0	0.30
DA	58.8	0.29
Die pad	121.0	0.33
BT epoxy	26.0	0.39
Solder mask	23.5	0.40
Solder balls	10.0	0.40
PCB	22.0	0.29

Table 3.3: Shear modulus for interfacial delamination stress intensity factor (Shin, D.K. et al., 1998, p.416)

Material	Shear modulus, μ (GPa)
MC (epoxy)	1.38
Die (silica)	30.6

During the study, the material properties was assumed to be linear (temperature and time independent) and homogenous. The interfaces between different components were also assumed to be perfectly contacted.

3.2 Theoretical applications of MCCI method

Fracture mechanics is the study of cracks or small flaws in a component under pressure loading and thermal loading. The maximum stress allowed can be determined if it contains acceptable and unavoidable cracks or delaminations without causing further damage to the component. Generally, fracture mechanics involves correlating analytical predictions of crack propagation by using energy criteria and stress criteria fracture theories. Energy criteria calculates strain energy release rate (SERR) in the crack region and stress criteria finds stress intensity factor (SIF) which is the magnitude of crack tip stress field.

In fracture mechanics, the crack resistance of material depends on several factors, outlined by Askeland, D.R. (1994). Larger crack reduces the permitted stress and create more possibility for crack to propagate. For ductile metals such as copper (Cu), the region near the crack tip can deform, causing the tip to be blunt, and yet preventing or delaying crack propagation. Rigid structural has lower fracture toughness than thin plate. Besides, cyclic and impact loading can cause fatigue before critical conditions. The temperature

may also affect its fracture toughness because different molecular energy absorption mechanisms active in different environments.

So, a lot of effort had been done by researchers to reduce the cracking and to improve crack resistance. Sauber, J. et al. (1994) mentioned that the ability of MC material to resist crack propagation depends on the chemical makeup of its resin system and the content, shape and size of the filler.

Finite element method (FEM) is useful as well as powerful in solving these linear elastic fracture mechanics (LEFM) problems. It is a numerical method of solving a system in governing equations over the domain of a continuous physical system. Small parts, called elements are subdivided into domain of the 2-D structure. The essence of the FEM is to take a complex problem such as package plastic failure, in which the solution may be difficult if not impossible to obtain and decompose it into pieces with simple approximate solutions, together to obtain a global approximate solution. The finite element (FE) approaches can be described by calculating the SERR and transforms it into SIF.

Rybicki, E.F. et al. (1977) stated that SERR can be defined in terms of the change in potential energy at crack tip, shown as follow;

$$G=\frac{d\psi}{da}-\frac{d\Phi}{da} \tag{3.1}$$

In Irwin's theory, if a crack extended by a small amount Δa, the energy absorbed in the process is equal to work required to close the crack to its original length, as mentioned in Rybicki, E.F. et al. (1977);

$$\begin{aligned} G = &\lim_{\Delta a\to 0}\frac{1}{2\Delta a}\int_0^{\Delta a}\sigma(\Delta a-r,0)v(r,\pi)dr \\ &+\lim_{\Delta a\to 0}\frac{1}{2\Delta a}\int_0^{\Delta a}\tau(\Delta a-r,0)u(r,\pi)dr \end{aligned} \tag{3.2}$$